Solid Freeform Fabrication 2018: Proceedings of the 29th Annual International Solid Freeform Fabrication Symposium – An Additive Manufacturing Conference
Reviewed Paper

Model Development for Residual Stress Consideration in Design for Laser Metal 3D Printing of Maraging Steel 300

Vedant Chahal and Robert M. Taylor

Department of Mechanical and Aerospace Engineering, The University of Texas at Arlington, Arlington, Texas 76010

Abstract

Design optimization of laser metal 3D printed structural components requires prediction of build-process induced residual stresses that vary with part geometry and affect distortion and support requirements during the build. Finite element residual stress state evaluation is not feasible within the computational constraints of iterative optimization. Alternatively, a simplified theoretical model is presented for predicting the residual stresses induced during Selective Laser Melting of maraging steel. Furthermore, a Design of Experiments (DOE) approach is implemented to verify the theoretical model and develop a response surface suitable for design optimization. The DOE uses cantilever geometry with length, thickness, and fillet radius as variables and shows overhang length to have the greatest influence on residual stresses. Geometries with high stiffness lead to lower deformations and tend to retain high stresses. The presented model can predict the trend of residual stresses for different geometries and can be used in shape optimization.

1 Introduction

Selective Laser Melting (SLM) is a layer by layer additive manufacturing (AM) process which produces high density parts with relatively good surface finish and has the capability to fabricate intricate structures up to 0.1 mm thickness [1], [2]. However, parts produced by SLM retains high residual stresses and could deform after separation from build plate, resulting in poor dimensional accuracy [3]. To account for these factors in part design, computationally lightweight design techniques are required which can precisely estimate the effect of part geometry on the resulting stresses and deformations. Many authors have worked on the finite element modeling of the SLM process and have successfully estimated induced residual stresses [4–6], however, these methods are computationally expensive and cannot be used in an iterative design process such as topology or shape optimization. Another approach is to experimentally develop a response surface for the geometric features which are to be optimized for induced stresses and distortions, as suggested by Taylor et al. [7].

To date, limited research has been performed on the stress characterization of maraging steel fabricated by SLM. It is well known that additive manufacturing of Ti6AL4V and AlSi10Mg leads to steep temperature gradients and high thermal shrinkage resulting in residual stresses which are tensile near the top and bottom surfaces and compressive in between [8]. However, parts made of maraging steel and H13 tool steel contain compressive stresses in top and bottom regions and tensile stresses in middle which can be attributed to martensite phase transformation resulting in volume expansion [9], [4]. AM fabricated maraging steel usually contains 90 to 95%

martensite (α) owing to the chemical composition of maraging steel and thermal stresses in added layers [10, 11]. High tensile stresses which are initially induced due to thermal shrinkage cause deformation-induced martensite transformation which stimulates the phase transformation well above martensite start temperature [12] and leads to high volume expansion [13].

This paper presents an analytical model for characterization of residual stress in additive manufacturing of Maraging Steel 300 by SLM. The model considers the layer-by-layer stress and strain development and can predict the trend of residual stresses for different process parameters and part geometries. Furthermore, resulting part deformation post base plate removal are evaluated by importing residual stress profiles predicted by the model into the Ansys APDL solver for mechanical analysis. Section 2 and 3 outlines the theoretical model and section 4 discusses the results of the model and compares them with a DOE study [7]. Section 5 summarizes the conclusions and discusses the future scope of this study.

2 Theoretical model

SLM is a powder bed fusion AM process where a blade or roller adds a layer of powdered material on top of a base plate which is scanned by a high intensity laser beam, heat energy from the laser melts the powder which rapidly solidifies owing to the high heat conductivity of the base plate. This process is repeated until part fabrication is complete. Macelis and Kruth [8] presented a simplified theoretical model for the SLM process assuming that thermal shrinkage of an added layer induces tensile stresses equivalent to yield strength of the material and a linear strain profile through the base plate-part combination. Force and moment equilibria are then used to calculate residual stress profile of the part-base plate combination. However, in the case of maraging steel as the added layer cools down and reaches martensite start temperature these tensile stresses aid in the phase transformation which is accompanied by volume expansion as shown in Figure 1a where the dilatometric loop for the cases when no load is applied and when tensile loads of 29 and 50 MPa are applied just before the martensite phase transformation [13]. This expansion is substantial enough to negate the tensile strain due to thermal shrinkage and induces compressive strain instead, as shown by Figure 1b.

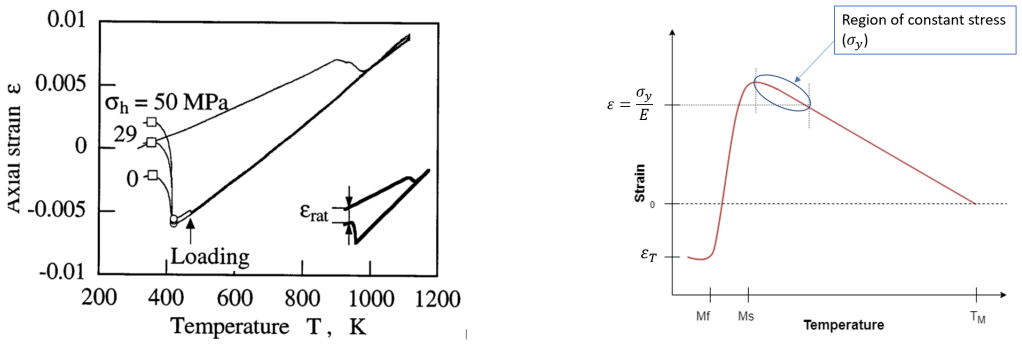

(a) (b)

Figure 1: (a) Dilatometric loop under applied stress [13], and (b) estimated strain development in added layer

The model presented here assumes a compressive strain ε_T in the added layer. Furthermore, supports are usually preferred to facilitate easy removal of the part from base plate and for overhang features and are thus added in the theoretical model. The model is based on strain energy, force, and torque equilibria along with the following assumptions to evaluate the stress and strain profiles within the part,

- Longitudinal stress (σ_{xx}) is independent of y coordinate,
- The general beam theory is valid,
- Added layers have a compressive strain (ε_T),
- No external forces are applied to the combination base plate-support-part, and
- A linear strain profile throughout the base plate, supports, and part.

Strain in added layer: K. Nagayama et al. [13] suggested that total strain due to martensite phase transformation at any given temperature is,

$$\varepsilon_T(T) = \varepsilon_{Ms} + \varepsilon_{trip} + (\delta/3)\zeta - (Ms - T)(\alpha_A(1-\zeta) + \alpha_M\zeta) \tag{1}$$

where, $\varepsilon_T(T)$ is the total strain at temperature T, ε_{Ms} is strain at martensite-start temperature, ε_{trip} is strain due to transformation induced plasticity, ζ is volume fraction of martensite, $\delta/3$ is eigen strain due to transformation where δ is transformation expansion, and α_A and α_M are coefficients of thermal expansion for austenite (parent) and martensite phase respectively. Furthermore, the magnitude of $\varepsilon_T(T)$ considerably depends on the applied stress and net volume expansion is higher for when tensile load is applied [13]. In the case of laser melting of maraging steel applied load at marteniste start temperature is equivalent to yield stress and drops rapidly once phase transformation begins. Hence a precise estimation of $\varepsilon_T(T)$ for the current study is not feasible. An initial estimate of $\varepsilon_T(T) = \sigma_y/3E_p$ is used for the theoretical model and is later calibrated from the results of a DOE study [7].

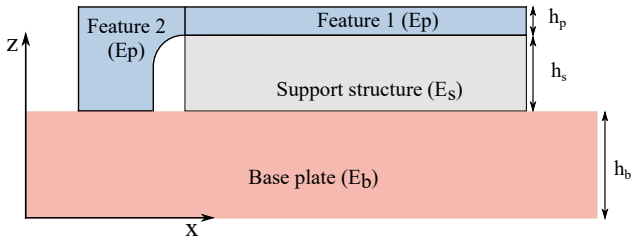

Figure 2: Part geometry

Strain profile: Figure 2 shows the part geometry, support structure orientation, and base plate dimensions used for the current study. A linear strain profile, $az + b$ over the base plate and $a_2(z - h_b) + b_2$ over the support structure and part combination is assumed, where a_2 is given by $a\,(E_b/E_s)$ and b_2 is simply $ah_b + b$, where h_b is height of the base plate, and E_b and E_s are effective elastic moduli of base plate and support structure respectively,

$$\varepsilon_b = az + b \tag{2}$$

$$\varepsilon_s = a\left(\frac{E_b}{E_s}\right)(z - h_b) + ah_b + b \tag{3}$$

and strain in part (ε_p) is evaluated from equation 4 and 5 layer by layer.

Strain energy conservation: newly added layers will induce a compressive strain (ε_T) which will lead to a very small deformation of the whole structure, as layer thickness is usually less than $100\,\mu\mathrm{m}$. Since the resulting deformation are very small it is assumed that strain energy of the base plate, support structure, part, and added layer is conserved before and after layer addition because conservation of strain energy requires that applied loads (strain in added layer) must be equivalent to the strain energy developed in a body as it deforms.

$$\frac{E_b}{2}\int_0^{hb}\varepsilon_b^2\,dz \;+\; \frac{E_s}{2}\int_{hb}^{hb+hs}\varepsilon_s^2\,dz \;+\; \frac{E_p}{2}\int_{hb+hs}^{hb+hs+hp}\varepsilon_p^2\,dz \;+\; \frac{E_p}{2}\,\varepsilon_T^2\,t \;=$$
$$\frac{E_b}{2}\int_0^{hb}\varepsilon'^2_b\,dz \;+\frac{E_s}{2}\int_{hb}^{hb+hs}\varepsilon'^2_s\,dz \;+\; \frac{E_p}{2}\int_{hb+hs}^{hb+hs+hp+t}\varepsilon'^2_p\,dz \tag{4}$$

where, E_p and E_b are Young's Moduli of part and base plate respectively, E_s is effective Young's Modulus of support structure in longitudinal (x) direction, ε_T is strain in added layer, ε_b, ε_s and ε_p are strains in base plate, support structure and part respectively, ε'_b, ε'_s and ε'_p are strains in base plate, supports structure and part after adding of new layer, and h_b, h_s, h_p, and t are height of base plate, supports, part and the added layer respectively.

Force and torque balance: since no external forces are applied to the whole structure, force and torque balance will always be maintained, as given by equation 5,

$$E_b\int_0^{hb}\varepsilon'_b\left(\frac{1}{z}\right)dz \;+\; E_s\int_{hb}^{hb+hs}\varepsilon'_s\left(\frac{1}{z}\right)dz \;+\; E_p\int_{hb+hs}^{hb+hs+hp+t}\varepsilon'_p\left(\frac{1}{z}\right)dz \;=\; 0 \tag{5}$$

3 Model implementation

Theoretical model discussed in previous section is used to predict the stress profile of the part shown in Figure 2. The part is divided in two features because the overhang (feature 1) is built on supports and has a uniform layer length whereas the radius (feature 2) is built directly on the base plate and its layer length changes with height. Stress evaluation for both features is carried out separately, this is possible as according to the model strain in any layer depends only on the stresses and stiffness of underlying material.

Stress profile for feature 1: to obtain the stress profile in the base plate-support-part combination, equation 2 to 5 are solved numerically for the following process parameters: $E_b = 200\,\mathrm{GPa}$, $E_s = 70\,\mathrm{GPa}$, $E_p = 160\,\mathrm{GPa}$, $h_b = 20\,\mathrm{mm}$, $h_s = 5\,\mathrm{mm}$, $h_p = 2\,\mathrm{mm}$, $t = 40\,\mu\mathrm{m}$, and $\varepsilon_T = -0.001875$. Furthermore, residual stress in the part after support removal is calculated by adding a relaxation stress ($pz + q$) to the stress profile of the part. Since force and torque balance have to be maintained post part separation, Equation 5 is solved again to evaluate the relaxation stress [8]. Figure 3a shows compressive stresses in the part which increase with the part height, tensile stresses in supports, and a linear profile of stress in the base plate, being compressive at bottom and tensile at the top. There is a sudden drop in residual stress magnitude from base plate

to support structure as the elastic modulus of supports is much lower than base plate. Figure 3b shows the residual stress profile in the part post separation from support structures. The part retains very low residual stresses owing to stress relaxation due to deformation of the part such that resulting stress profile is compressive at the top and bottom regions and tensile in between.

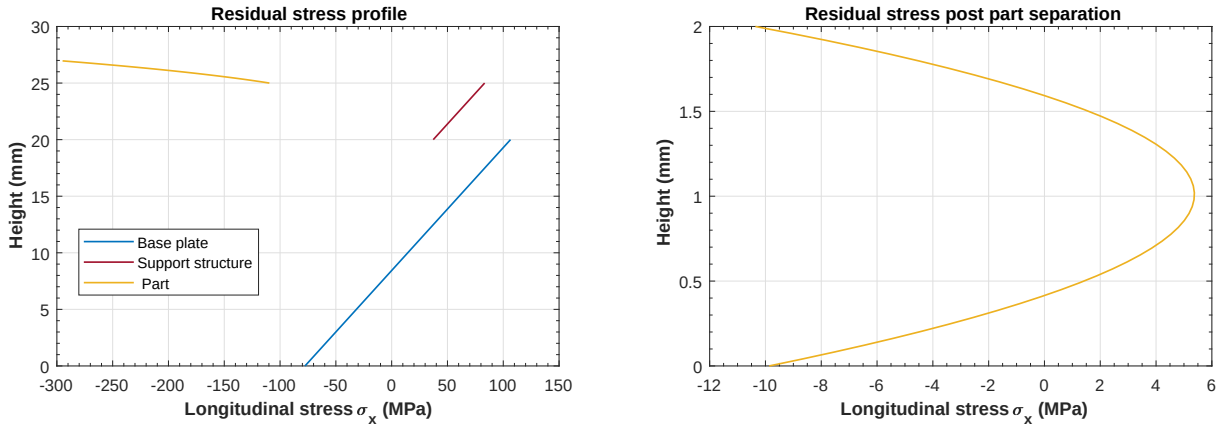

(a) (b)

Figure 3: Residual stress profile (a) before support removal and (b) after support removal

Stress profile for feature 2: to use the same theoretical model for this feature, we need to account for the increase of layer length in Equation 4 and 5 as the part grows in height. As shown in Figure 4b, ΔL part of added layer is free to deform and does not contribute to the strain profile of the part, to accommodate that, stiffness ($E_{b(n)}$) of layer n is changed to $E_b(L_{n-1}/L_0)$, where L_{n-1} is the length of layer $n-1$ and L_0 is the initial length of the part as shown in Figure 4a. The length of layer n at any height h is given as,

$$L_n = L_0 + (R - \sqrt{R^2 - (h - h_1)^2}) \tag{6}$$

where, R is the radius of the fillet and h_1 is the part height at which the fillet begins. However, once this layer solidifies and another layer is added on top, the stiffness of the whole layer has to be considered i.e. $E_{b(n)}$ should be $E_b(L_n/L_0)$.

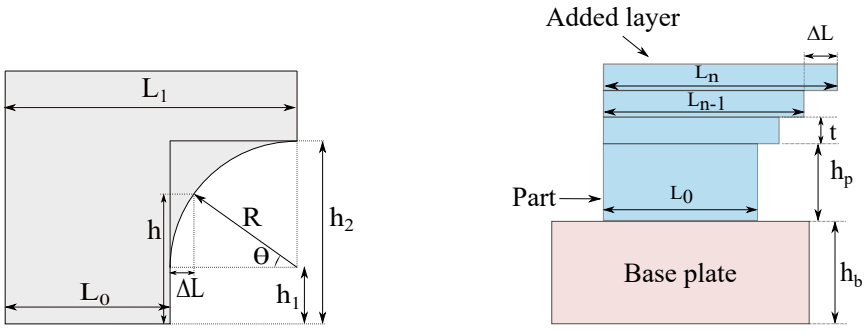

(a) (b)

Figure 4: Mathematical modeling of fillet (feature 2)

Figure 5 shows the residual stress profile with in the part and base plate. Process parameters similar to that of previous case were used except for part height of 7 mm, fillet radius of 4 mm, $h_1 = 1\,\text{mm}$, and $L_0 = 5\,\text{mm}$ were taken as geometric dimensions.

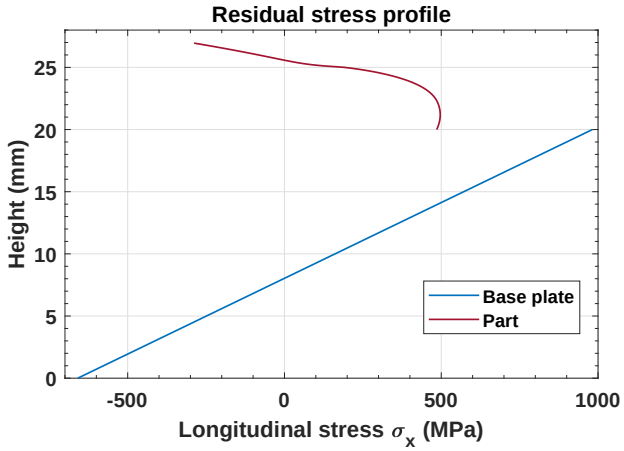

Figure 5: Residual stress profile for feature 2 before part separation

4 Results

The Influence of certain process parameters on AM induced residual stresses were evaluated from the theoretical model. The stress profiles obtained from the model were used to estimate part deformations which were then compared with the results obtained from a DOE study conducted by Taylor et al. [7].

4.1 Theoretical model

Figures 6 to 12 shows the stress profiles obtained from the model. Process parameters used: $E_b = 200\,\text{GPa}$, $E_s = 70\,\text{GPa}$, $E_p = 160\,\text{GPa}$, $h_b = 20\,\text{mm}$, $h_s = 5\,\text{mm}$, $h_p = 2\,\text{mm}$, $t = 50\,\mu\text{m}$, $\varepsilon_T = -0.001875$.

Figure 6a shows the residual stress profiles of the part, support, and base plate and Figure 6b shows the residual stress profile of part post support removal for effective support stiffness of 40, 80, and 120 GPa. It can be observed that longitudinal stiffness of support structure has a significant effect on the residual stress profile of the part and would consequently affect the part distortion after support removal. Figure 7 shows the influence of base plate stiffness. However, if supports are used then base plate stiffness has a minimal influence of the stress profiles as shown in Figure 8. Figure 9 shows the influence of part height, as the part grows in thickness, residual stresses retained post part removal increases and so does the stresses in base plate and support structure. As the part grows in height, supports and base plate could deform plastically making it difficult to analyze the stress profile for overhang geometries with height greater than 4 mm. Figure 12 shows the effect of fillet radius used in feature 2 (shown in Figure 2). For the stress evaluation of feature 2 similar process parameters as before were used except for the total part height of 7 mm and part height of 2 mm above the fillet were used.

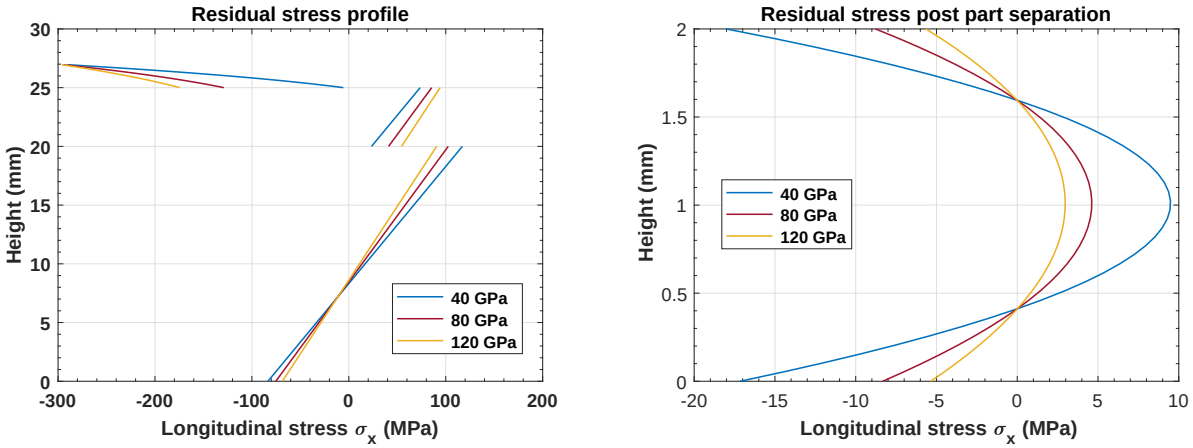

(a) (b)

Figure 6: Stress profiles for effective support structure stiffness of 40, 80, and 120 GPa

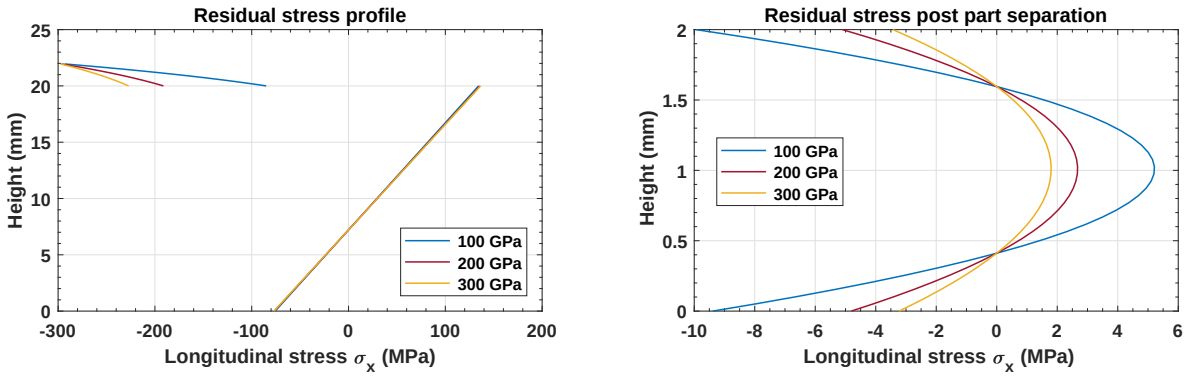

(a) (b)

Figure 7: Stress profiles for base plate stiffness of 100, 200, and 300 GPa (without supports)

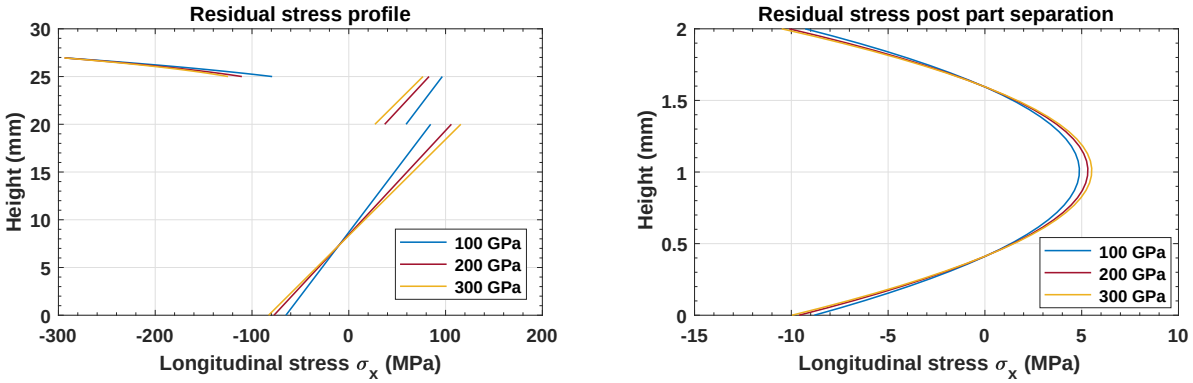

(a) (b)

Figure 8: Stress profiles for base plate stiffness of 100, 200, and 300 GPa (with supports)

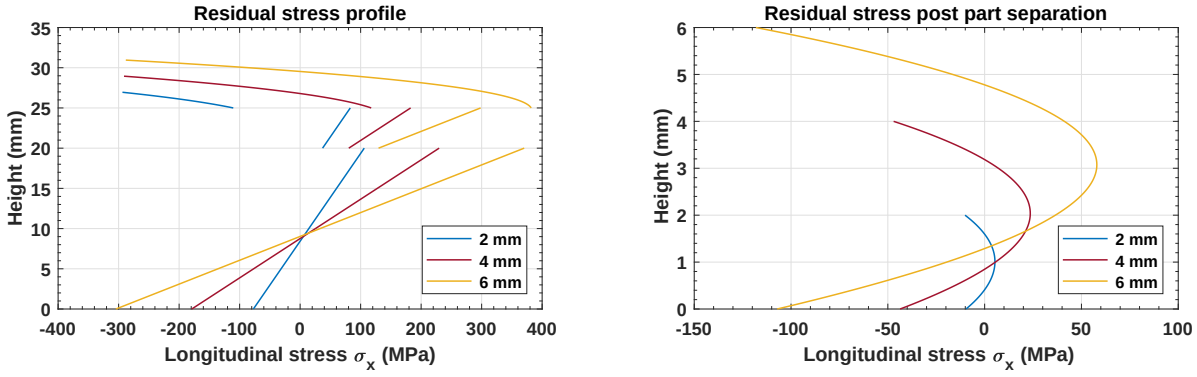

(a) (b)

Figure 9: Stress profiles for part height of 2, 4, and 6 mm

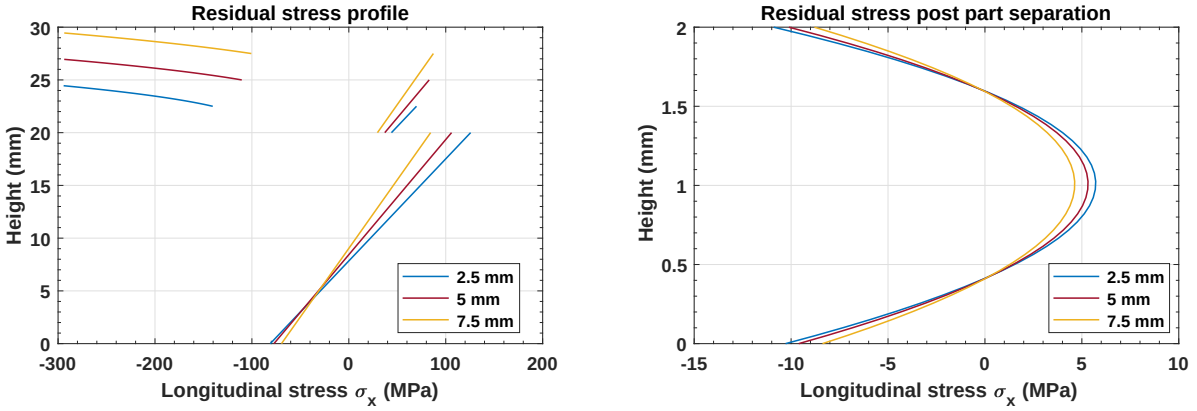

(a) (b)

Figure 10: Stress profiles for support structure height of 2.5, 5, and 7.5 mm

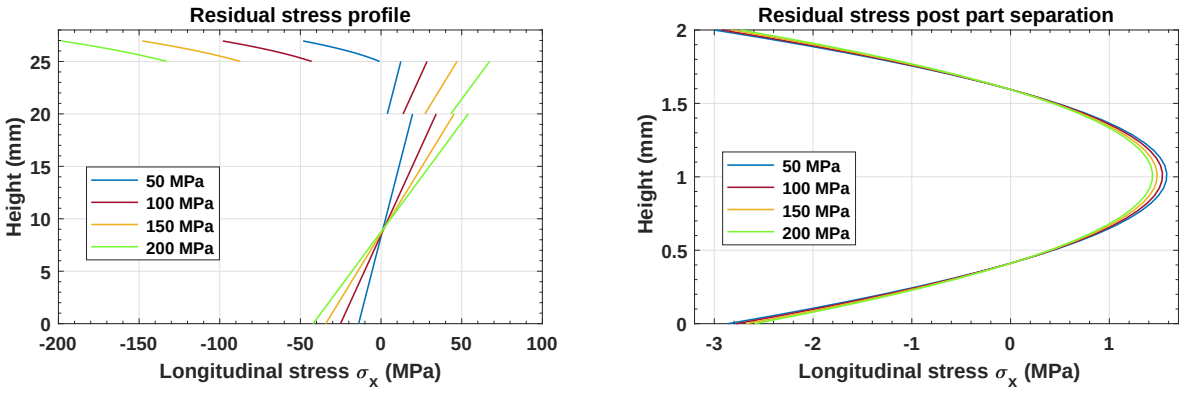

(a) (b)

Figure 11: Influence of induced stress ($\varepsilon_T \times E_p$) in added layer

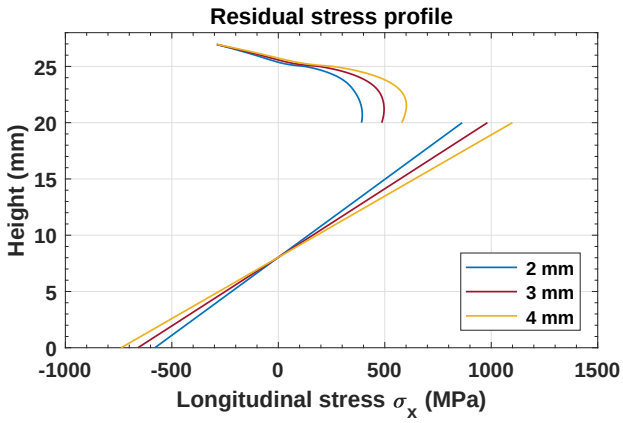

Figure 12: Stress profiles for fillet radii of 2, 3, and 4 mm

4.2 Design of Experiments

Results of DOE study conducted by Taylor et al. [7] were used to validate the theoretical model where an overhang geometry similar to Figure 2 was used to conduct a 3 factor 2 level, full factorial DOE [7]. Figure 13 shows the overhang specimen used for the DOE study before and after support removal. Table 1 lists the specimen dimensions and results of the study. Influence of all three features on the end deflection of the overhang feature is given by Equation 7,

$$Def(A,\, B,\, C) = (-3.52 + 0.92A - 1.81B - 0.23C + 0.09AB + 0.29AC - 0.29BC + 0.23ABC) \times 10^{-2} \quad (7)$$

where, A is overhang thickness, B is overhang length, and C is fillet radius. To evaluate overhang deflection residual stress profiles predicted by the model were imported into Ansys APDL as initial state of the elements using the inistate command of the APDL solver. The theoretical model was initially calibrated for the strain in added layer (ε_T). The First specimen was used to evaluate ε_T and the predictions of the end deflection for all the other specimens are listed in Table 1.

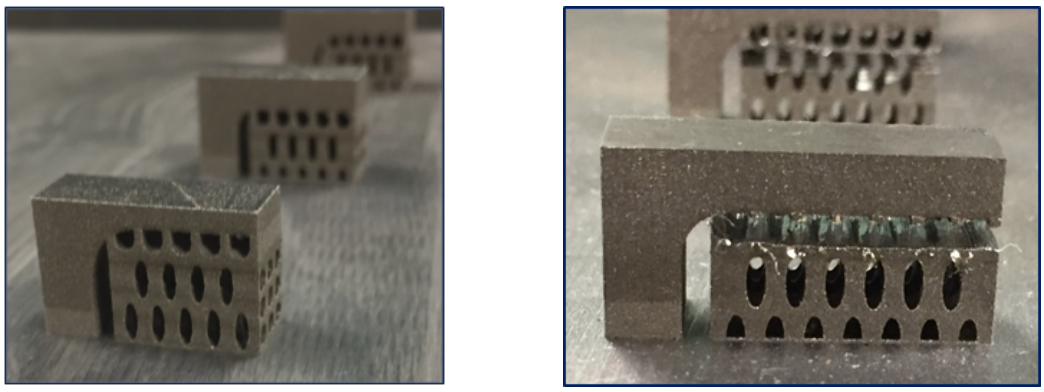

(a) (b)

Figure 13: Overhang feature specimen (a) as built and (b) post support removal [7]

DOE results for parts with a thickness of 4 mm show much lower distortion, it is likely due to localized stress concentration in the support structures resulting in plastic strain which could

lead to stress relaxation within the part. Since the model only considers longitudinal stresses and does not account for variation in thermal conductivity with part geometry, precise estimation of the resulting distortion and residual stresses is not feasible. However, qualitative effect of geometric features on residual stresses and distortions can be predicted. If a uniform support geometry was used in the DOE study, results from the theoretical model would be more comparable, as strain profile over the support structure height would be consistent. Furthermore, cyclic thermal loading of underlying layers as new layers are scanned by the laser could lead to stress relaxation which is not considered in the theoretical model.

Table 1: Results from theoretical model and DOE

Overhang Length (mm)	Fillet radius (mm)	Thickness (mm)	End Deflection (mm)	
			DOE	Theoretical model
20	3	2	-0.053	-0.053
15	3	2	-0.025	-0.027
20	5	2	-0.074	-0.057
15	5	2	-0.025	-0.029
20	3	4	-0.043	-0.060
15	3	4	-0.010	-0.030
20	5	4	-0.043	-0.068
15	5	4	-0.008	-0.035

5 Conclusions

A theoretical model has been presented that adds the effect of martensite phase transformation in maraging 300 steel to previously developed residual stress predictive models. This model can be effectively used to predict the influence of various process parameters and part geometry on residual stress profiles within the part before and after separation from the base plate for additive manufacturing of maraging steel.

The model suggests that stiffness of supports in longitudinal direction plays a vital role in the resulting residual stresses and part distortions post support removal. Weaker support structures are usually preferred for additive manufacturing to facilitate easy removal and to avoid material wastage however, current study illustrates that such supports will lead to high residual stresses and lower dimensional accuracy. Similar results were obtained by Hussein et al. [14] where different lattice structures, their manufacturability, and effect on part distortion were studied.

Much future work remains and is planned to further develop this model to include the influence of stress relaxation due to cyclic thermal loading as further layers are scanned on top. For the residual stress experiment, factor levels will be refined to explore realistic limits. Support structure configuration factors will be added to include the effect of support stiffness on residual stress development. Further, residual stress in the, as-built and post support removal, DOE specimens will be measured for the validation of proposed model.

Acknowledgments

The authors appreciate the support from Advanced Graphic Systems for 3D printing the DOE specimens.

References

[1] F. Wang, "Mechanical property study on rapid additive layer manufacture hastelloy® x alloy by selective laser melting technology," *The International Journal of Advanced Manufacturing Technology*, vol. 58, no. 5-8, pp. 545–551, 2012.

[2] L. Mullen, R. C. Stamp, W. K. Brooks, E. Jones, and C. J. Sutcliffe, "Selective laser melting: A regular unit cell approach for the manufacture of porous, titanium, bone in-growth constructs, suitable for orthopedic applications," *Journal of Biomedical Materials Research Part B: Applied Biomaterials*, vol. 89, no. 2, pp. 325–334, 2009.

[3] R. Paul, S. Anand, and F. Gerner, "Effect of thermal deformation on part errors in metal powder based additive manufacturing processes," *Journal of Manufacturing Science and Engineering*, vol. 136, no. 3, p. 031009, 2014.

[4] M. F. Zaeh and G. Branner, "Investigations on residual stresses and deformations in selective laser melting," *Production Engineering*, vol. 4, no. 1, pp. 35–45, 2010.

[5] I. A. Roberts, C. Wang, R. Esterlein, M. Stanford, and D. Mynors, "A three-dimensional finite element analysis of the temperature field during laser melting of metal powders in additive layer manufacturing," *International Journal of Machine Tools and Manufacture*, vol. 49, no. 12-13, pp. 916–923, 2009.

[6] N. Hodge, R. Ferencz, and J. Solberg, "Implementation of a thermomechanical model for the simulation of selective laser melting," *Computational Mechanics*, vol. 54, no. 1, pp. 33–51, 2014.

[7] R. M. Taylor and V. Chahal, "A framework for robust lightweight structural design for additive manufacture," *Advances in Aerospace Structures, Systems and Technology, London, UK*, 2018.

[8] P. Mercelis and J.-P. Kruth, "Residual stresses in selective laser sintering and selective laser melting," *Rapid prototyping journal*, vol. 12, no. 5, pp. 254–265, 2006.

[9] R. Cottam, J. Wang, and V. Luzin, "Characterization of microstructure and residual stress in a 3d h13 tool steel component produced by additive manufacturing," *Journal of Materials Research*, vol. 29, no. 17, pp. 1978–1986, 2014.

[10] K. Kempen, E. Yasa, L. Thijs, J.-P. Kruth, and J. Van Humbeeck, "Microstructure and mechanical properties of selective laser melted 18ni-300 steel," *Physics Procedia*, vol. 12, pp. 255–263, 2011.

[11] C. Tan, K. Zhou, W. Ma, P. Zhang, M. Liu, and T. Kuang, "Microstructural evolution, nano-precipitation behavior and mechanical properties of selective laser melted high-performance grade 300 maraging steel," *Materials & Design*, vol. 134, pp. 23–34, 2017.

[12] S. Y. Zhang, E. Compagnon, B. Godin, and A. M. Korsunsky, "Investigation of martensite transformation in 316l stainless steel," *Materials Today: Proceedings*, vol. 2, pp. S251–S260, 2015.

[13] K. Nagayama, T. Terasaki, K. Tanaka, F. Fischer, T. Antretter, G. Cailletaud, and F. Azzouz, "Mechanical properties of a cr–ni–mo–al–ti maraging steel in the process of martensitic transformation," *Materials Science and Engineering: A*, vol. 308, no. 1-2, pp. 25–37, 2001.

[14] A. Hussein, L. Hao, C. Yan, R. Everson, and P. Young, "Advanced lattice support structures for metal additive manufacturing," *Journal of Materials Processing Technology*, vol. 213, no. 7, pp. 1019–1026, 2013.